Journal of Geophysical Research: Oceans

RESEARCH ARTICLE
10.1002/2017JC013579

Wind Stress Mediated Variability of the Filchner Trough Overflow, Weddell Sea

K. Daae[1], E. Darelius[1], I. Fer[1], S. Østerhus[2], and S. Ryan[3]

[1]Geophysical Institute, University of Bergen and Bjerknes Centre for Climate Research, Bergen, Norway, [2]Uni Research Climate, and Bjerknes Centre for Climate Research, Bergen, Norway, [3]Alfred Wegener Institute, Helmholtz Centre for Polar and Marine Research, Bremerhaven, Germany

Key Points:
- Ice Shelf Water overflow is related to wind variability along the continental slope upstream of Filchner Trough
- Monthly scale variability in the slope current and Antarctic Coastal Current is strongly linked to the alongslope wind variability

Supporting Information:
- Supporting Information S1
- Figure S1
- Figure S2
- Figure S3
- Figure S4
- Figure S5
- Figure S6
- Table S1
- Movie S1

Correspondence to:
K. Daae,
kjersti.daae@uib.no

Citation:
Daae, K., Darelius, E., Fer, I., Østerhus, S., & Ryan, S. (2018). Wind stress mediated variability of the Filchner Trough Overflow, Weddell Sea. *Journal of Geophysical Research: Oceans*, *123*, 3186–3203. https://doi.org/10.1002/2017JC013579

Received 25 OCT 2017
Accepted 21 MAR 2018
Accepted article online 26 MAR 2018
Published online 6 MAY 2018

Abstract The Filchner Trough (FT) is a key site for exchange of water masses between the Weddell Sea continental shelf and the deep ocean. Cold and dense Ice Shelf Water (ISW), a precursor for Antarctic Bottom Water, flows north along the FT and overflows the Filchner Sill. Although access of warm water to the Weddell Sea continental shelf is limited due to the presence of the Antarctic Slope Front, southward transport of warm water is facilitated through the FT. We use moored current meters from the Filchner Sill region to show that the monthly scale variability of the ISW overflow is connected to the variability of the alongslope wind stress upstream. Periods with significant correlation between the wind and ISW overflow are characterized by (I) wind directed along the continental slope, (II) high ISW overflow speed, and (III) high variability in the 16–64 day period band for wind and current. We propose that a recirculation of the slope current, associated with the Antarctic Slope Front, may occur in the FT during periods of strong wind forcing, and that such recirculation could explain the correlation between the wind stress and the ISW overflow. We further show that an increased wind stress along the continental slope leads to increased current speed within the slope current and the Antarctic Coastal Current, with possible implications for the on-shore heat transport.

1. Introduction

The southeastern Weddell Sea is a site of climatic importance, where exchanges of water masses between the shallow continental shelf and the deep ocean occur. In deeper layers, cold and dense Ice Shelf Water (ISW), formed through interaction between High Salinity Shelf Water (HSSW) and the Filchner-Ronne Ice Shelf cavity, exits the Filchner Trough (FT, map in Figure 1) and contributes to the formation of Antarctic Bottom Water (AABW) (Darelius et al., 2009; Foldvik et al., 2004), which is an important driver of the global thermohaline overturning circulation. In the upper layers, Warm Deep Water (WDW), a slightly cooler and fresher derivative of the Circumpolar Deep Water (Heywood et al., 1998), enters the shelf and may contribute to increasing the mass loss of the floating ice shelves through basal melting (Hellmer et al., 2012). At present climate, the water temperature on the Weddell Sea shelf is low (near freezing point) and the ice shelf melt rates are low compared to, e.g., the Amundsen Sea (Pritchard et al., 2012; Rignot et al., 2013).

The access of WDW onto the shelf is limited by the Antarctic Slope Front (ASF), which separates the WDW from the cold and fresh Eastern Surface Water (Gill, 1973; Jacobs, 1991). The ASF is largely wind-driven. The slope current, associated with the ASF, carries WDW westward along the continental slope. On interannual time scales, the variability of the slope current is connected to the wind-driven Weddell gyre (Gordon et al., 2010), and on seasonal time scales the slope current corresponds well with easterly wind along the continental slope (Fahrbach et al., 1992; Graham et al., 2013). Maximum slope current transport is found during austral winter (May–July) when the wind forcing is strong and the slope current is barotropic (Núñez-Riboni & Fahrbach, 2009).

Modified Warm Deep Water (MWDW, $\theta > -1.7$°C), a slightly cooled version of WDW, crosses the shelf break and enters the continental shelf seasonally (January–May) (Årthun et al., 2012; Ryan et al., 2017), when weaker wind forcing allows for a shoaling of the thermocline. Recent observations near the Filchner Ice Shelf (FIS) front (Darelius et al., 2016) show that when WDW is present on the shelf, strong wind from northeast can advect this water mass southward toward the FIS front. Furthermore, numerical modeling results

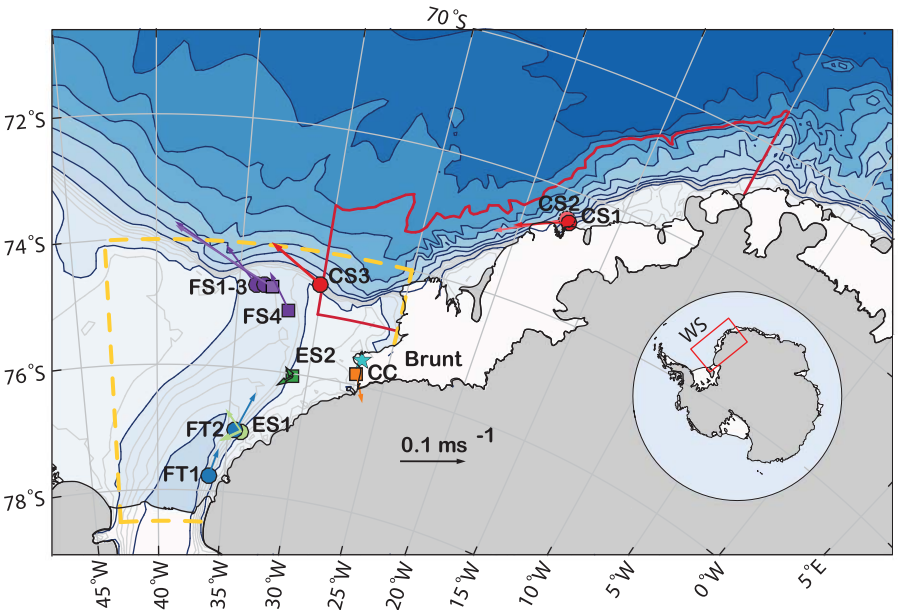

Figure 1. Map showing the Southeastern Weddell Sea (WS) bathymetry and the mooring locations. Color coding and mooring names refer to Continental Slope (CS, red), Coastal Current (CC, orange), Eastern Shelf (ES, green), Filchner Trough (FT, blue), and Filchner Sill (FS, purple). Squares indicate mooring records of 2–3 years duration, while circles indicate year-long records. Colored arrows from each mooring location show vector mean currents. At FS1 and FS2 we show mean currents from 1977 and 2010, respectively. At ES1–2, the current direction changes seasonally, and we show two vectors, representing mean currents during inflow and cross-flow periods. The turquoise star on the Brunt Ice Shelf shows the location of the Halley Research Station. ERA upstream Wind and SIC are extracted from the region bounded by the red line and the coast. Additional SIC is extracted from the Filchner region delineated by the yellow dashed line.

(Hellmer et al., 2012, 2017; Timmermann & Hellmer, 2013) predict that the slope current carrying warm water could be redirected southward, in the near future.

The cross-shelf FT plays a key role in facilitating the transport of MWDW toward the FIS. Warm water ($\theta > -1.9$°C), with a core at 400 m depth, is observed along the eastern flank of the FT in several hydrographic surveys (Årthun et al., 2012; Carmack & Foster, 1977; Darelius et al., 2014a; Foldvik et al., 1985a; Ryan et al., 2017). Interactions between a shelf break jet and a cross-shelf trough depend on the trough geometry, stratification, and the strength and direction of the flow (Allen & Durrieu de Madron, 2009; Klinck, 1996; Williams et al., 2001; Zhang et al., 2011). Results from an idealized numerical model showed that the inflow of warm water in the FT strongly depends on the wind forcing due to associated changes in the slope current (Daae et al., 2017). A sketch of the slope current, based on the idealized model results, for weak and strong wind forcing is given in Figure 2. During weak winds, the slope current crosses the FT opening, and the water exchange between the slope and the FT is dominated by eddies. During strong winds, a shoreward, wind-driven branch of the slope current is steered south into the FT, bringing warm water into the region. Due to potential vorticity constraints near the southern sill edge (where the FT is getting deeper), the current recirculates and exits the FT toward the west.

Here we explore the connections between wind and current circulation associated with the ISW overflow and the ASF processes in the southeastern Weddell Sea on a monthly time scale. We use several year-long current records from moored instruments on the continental slope and shelf region, as well as from the FT (Figure 1).

We present new findings of a high correlation between the ISW overflow from FT and the alongslope wind upstream. We propose a mechanism that could explain such high correlation. If the wind-forced slope current recirculates at the mouth of the FT, as suggested by the idealized model results (Daae et al., 2017) (Figure 2), interactions between the slope current and the ISW overflow could increase the overflow speed. Although the existing data set is insufficient to prove the mechanism, we present measurements at different locations which are consistent with the proposed recirculation of the slope current.

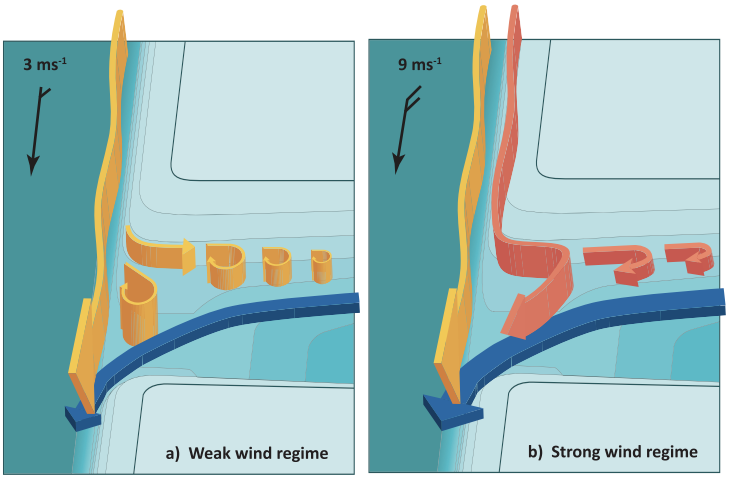

Figure 2. Sketch of the circulation over the Filchner Sill from idealized numerical simulations (Daae et al., 2017) with (a) weak wind along the slope, and (b) with strong wind along the slope. The continuous yellow arrows indicate the background slope current. During weak wind, the slope current flows across the FT opening, and eddies carrying moderately warm water (−1 to −1.5°C) enter the FT on its eastern flank. In the strong wind regime, a wind-driven slope current (red arrow) adds to the background current. We refer to this current as the Recirculating Slope Current (RSC). RSC circulates over the Filchner sill region, and leaves the Sill along with the dense Filchner overflow (blue arrow).

2. Data and Methods

2.1. Atmospheric Data

Atmospheric data are obtained from the ERA-Interim reanalysis data set with 0.75° resolution (Dee et al., 2011) (named ERA hereafter). The ERA data set has a time resolution of 6 h, and is available from 1979 to present. We extract ERA wind velocity at 10 m above sea level (mabsl). Wind stress is calculated following the procedure by Andreas et al. (2010), where the drag coefficient is a function of the Sea Ice Concentration (SIC). We use the SIC available in ERA to be consistent with the data set and grid for wind velocity. The coordinate system for wind stress is rotated, with the along-flow component directed toward 245°, roughly along the continental slope. Hereafter, this wind direction is referred to as the alongslope wind.

At monthly time scales, the pressure system governing the winds over the Weddell Sea is larger than our study region, yielding a similar wind pattern in the FT and over the continental slope. To illustrate this, a video of 15 days low-passed mean sea level pressure and wind vectors from 1995 is included in the supplementary material. We expect that the wind-driven slope current variability affects the on-shelf transport of water, and possibly the recirculation in the FT. Thus, we compare observed current speed to mean alongslope wind stress from an area over the continental slope, upstream of the FT, from 10°W–30°W to 69°S–75°S, limited by the 3,500 m isobath and the coastline (indicated by the red line in Figure 1). We refer to this region as the upstream region hereafter. Maps of correlation between along-flow current speed and wind speed (not shown), showed highest correlation for the continental slope region upstream along 245°, and support our choice of area and direction of wind stress used in further analysis.

The first current record from the Filchner Sill is from 1977, when neither ERA data nor SIC is available. To include this data set in our analysis, we instead compare the current speed with observed alongslope (245°) wind speed from the Halley Research station (British Antarctic Survey, 2013), located on the Brunt Ice Shelf (star in Figure 1). Fifteen day low-passed alongslope wind speed from ERA (upstream region) and Halley agree well ($R = 0.82$, above the 99% confidence limit, see section 2.4 for description of low-pass filtering and correlation analysis). For current records where ERA is available, correlations between the current speed and the ERA wind stress/Halley wind speed are similar.

There is a bias in the ERA and Halley time series. Low-passed, along-flow mean wind speed from Halley and ERA (1979–2017) are 3.3 and 1.9 m s^{-1}, respectively. However, we focus on the variability of the wind, and the difference in mean wind speed should not impact the results. To facilitate comparison of results from

moorings on the Filchner Sill, all figures from these locations show results for both Halley wind speed and ERA wind stress.

Correlation between current speed and wind from Halley is performed using wind speed, and not wind stress, since SIC is not available for all record years. From ERA data, correlations with current speed were similar using either wind speed or wind stress. We therefore assume that correlation values obtained using the Halley wind speed is representative for wind stress.

The sampling interval for Halley data was 3 h prior to 1986, and then increased to 1 h. Short periods of missing data are linearly interpolated prior to frequency analysis and low-pass filtering.

2.2. Sea Ice Concentration

Time series of SIC from 1978 to 2017 are extracted from the National Snow and Ice Data Center, (Cavalieri et al., 1996). The data set is a satellite product generated from brightness temperature on a 25 km $\times$ 25 km grid. While SIC from ERA is based on different data sets of sea surface temperature prior to 2009 (Dee et al., 2011), the NSIDC SIC product is consistent throughout the time series. We calculate daily (every 2 days prior to July 1987) mean SIC for the upstream area (same as for ERA wind), as well as for the Filchner region (marked by red/yellow in Figure 1, respectively). Mean summer SIC is calculated for the period December–February every year. The year 1988 is left out of the summer mean calculation due to missing SIC data in December 1987 and January 1988.

2.3. Moored Instruments

We analyze current records of 1–3 years duration from 14 moored instruments in the southern Weddell Sea (Figure 1). To facilitate the reading and the discussion of the moorings, we rename the moorings according to their locations: the Continental Slope (CS), the Coastal Current inflow (CC), the shelf area east of FT (ES), the Filchner Trough (FT), and the Filchner Sill (FS). An overview of the current records and measurement depth used in this document is given in Table 1. Mooring names used in earlier publications are given in brackets. A complete table of the moorings with available depths and instrument types is given in the supporting information.

The coordinate system at each mooring is rotated to the main flow direction, calculated from vector averaged currents (see Table 1). For moorings where the current changes seasonally (ES1–2 and FT1–2), we rotate the coordinates according to the bathymetry, roughly correspond to NE direction. The current along this direction is referred to as outflow. The defined along-flow direction at each current meter, is given in Table 1.

At the Filchner Sill, mooring records are available from three locations. The earliest record is from 1977 at FS1 and the latest record covers 2014–2016 at FS3. We omit three mooring records in this study. At FS1, we omit the 1987 record, since a large, stranded iceberg caused circulation changes of HSSW in the Filchner region (Darelius et al., 2014b; Grosfeld et al., 2001; Nøst & Østerhus, 1998). At FS2, we omit current records from 2009, where the data set is incomplete, and from 2014, where the current meter is higher up in the water column compared to the other FS moorings. The mooring FS4 is located just south of the Filchner Sill (see map in Figure 1), but is included in the FS group.

Potential densities (σ_Θ) on the continental slope are calculated according to TEOS-10 (IOC et al., 2010), using Absolute Salinity, and Conservative Temperature. Otherwise, we use potential temperatures referenced to surface (θ), since joint salinity measurements required to calculate Conservative Temperature, do not exist for all measurement depths and records.

2.4. Low-Pass Filtering, Correlations, and Wavelet Analysis

Wind and current data are low-pass filtered using 15 days moving Hanning windows (Lilly, 2017). The data series are zero-padded at each end to display data for the whole time series. We choose to study 15 day low-passed data in order to filter out the high-frequency variability such as tides, continental shelf waves, and short storm events.

Time series of correlation coefficients are calculated using moving windows of low-pass filtered alongslope ERA wind stress, or Halley wind speed, and current speed. For each window, we calculate normalized correlation and significance, following Sciremammano (1979), while allowing for up to 7 days lag. The method requires more than 10 degrees of freedom (dof). Dof is a function of the auto-correlation of each data series,

Table 1
Overview of the Mooring Records

Mooring name	Year	# days	Latitude (°S)	Longitude (°W)	Dir (°)	Bottom depth (m)	Current depth (m)	R wind/ curr.	Lag (days)	Reference
FS1 (S2)	1977	411	74° 40′	33° 56′	314	558	533	0.52^{99a}	1.00	Foldvik et al. (1985b)
FS1 (S2)	1985	371	74° 40′	33° 56′	322	545	520	0.33^{95}	0.75	Foldvik et al. (2004)
FS2 (S2)	2003	747	74° 40′	33° 28′	294	597	497	0.05^{NS}	7.00	Darelius et al. (2014b)
	2004							0.24^{90}	0.00	
FS2 (S2)	2010	364	74° 38′	33° 30′	281	602	577	0.13^{NS}	0.00	Darelius et al. (2014b)
FS3 (S2E)	2014	1124	74° 40′	33° 00′	296	593	580	0.28^{90}	2.25	
	2015							0.15^{NS}	0.75	
	2016							0.12^{NS}	0.25	
FS4 (FR1)	1995	837	75° 01′	31° 46′	326	610	484	0.47^{99}	0.75	Woodgate and
	1996							0.26^{90}	0.00	Schröder (1998)
	1995	829			336		257	0.34^{99}	0.5	
	1996							0.33^{95}	0.5	
FT1 ($M78_{7E}$)	2013	376	77° 45′	36° 09′	17	705	486	0.32^{NS}	7.00	Darelius et al. (2016)
FT2 ($M77_{7}$)	2013	371	77° 00′	34° 28′	35	705	382	0.14^{NS}	7.00	Darelius et al. (2016)
ES1 ($M77_{5}$)	2013	371	77° 00′	34° 03′	35	505	434	0.32^{NS}	7.00	Darelius et al. (2016)
ES2 (M_{31W})	2014	746	76° 00′	31° 00′	45	457	437	-0.06^{NS}	7.00	Ryan et al. (2017)
	2015							-0.17^{NS}	6.50	
CS1 (M1)	2009	386	72° 29′	17° 28′	245	273	224	0.69^{99}	0.50	Graham et al. (2013)
CS2 (M2)	2009	386	72° 27′	17° 38′	238	487	224	0.43^{95}	0.75	Graham et al. (2013)
					238		400	0.46^{99}	0.50	
CS3 (M3)	2009	361	74° 31′	30° 10′	301	725	220	0.54^{95}	5.50	Jensen et al. (2013)
					315		400	0.35^{90}	7.00	
CC (B3)	2003	746	75° 49′	26° 52′	158	392	194	0.60^{99}	3.25	Nicholls (2005)
	2004							0.47^{99}	1.75	

Note. Original mooring names are given in brackets. Correlation coefficients between the alongslope wind stress upstream of FT (see map in Figure 1) and the along-flow current speed from each mooring are given in column nine. Most current records cover roughly one year of data. In order to compare correlation coefficients between the records, we divide time series from moorings covering more than 2 years into sets of single years, including 13 months of data, from January to January. The significance level which is exceeded for the normalized correlation coefficients are indicated by superscripts. Nonsignificant correlations are marked by superscript NS. [a]Correlation with Halley alongslope (245°) wind speed.

and is high when the variability within each time series is high. For CS1–3, dof is too low to calculate running correlations. For CC, we obtain >10 dof using window lengths of 150 days, and for FT1–2 we obtain >10 dof for window lengths of 120 days. Moorings at ES and FS have higher internal variability and yield >10 dof for window lengths of 100 days.

Significance levels are denoted by upper superscripts (i.e., $R=0.6^{99}$ means that R is above the 99% significance level). In Table 1, correlation coefficients which do not exceed the 90% significance level are denoted by NS (Nonsignificant).

Complex wavelet transforms, X_ω, are computed for daily low-passed alongslope wind and the along-flow current speed using the Morlet wavelet. The wavelet basis is normalized to have energy power equal to one at all scales, and we apply zero-padding to prevent wraparound effects. The wavelet power is the modulus of the complex wavelet transform, $|X_\omega|$. It shows when energetic oscillations take place, and at what time scales they appear. The wavelet amplitude, which we will study here, is the real part of the wavelet transform, $\mathrm{Re}(X_\omega)$, and is a useful measure when we compare two time series. Whereas the wavelet power only shows when, and at what frequencies energetic oscillations occur, comparison of positive and negative states of the wavelet amplitudes from two time series can tell us when the two oscillations are in or out of phase (Cooper & Cowan, 2008).

3. Results

In this section, we first present the variability in the atmospheric forcing and the SIC (section 3.1). We then describe the relation between wind and current at different geographic locations, starting with the ISW

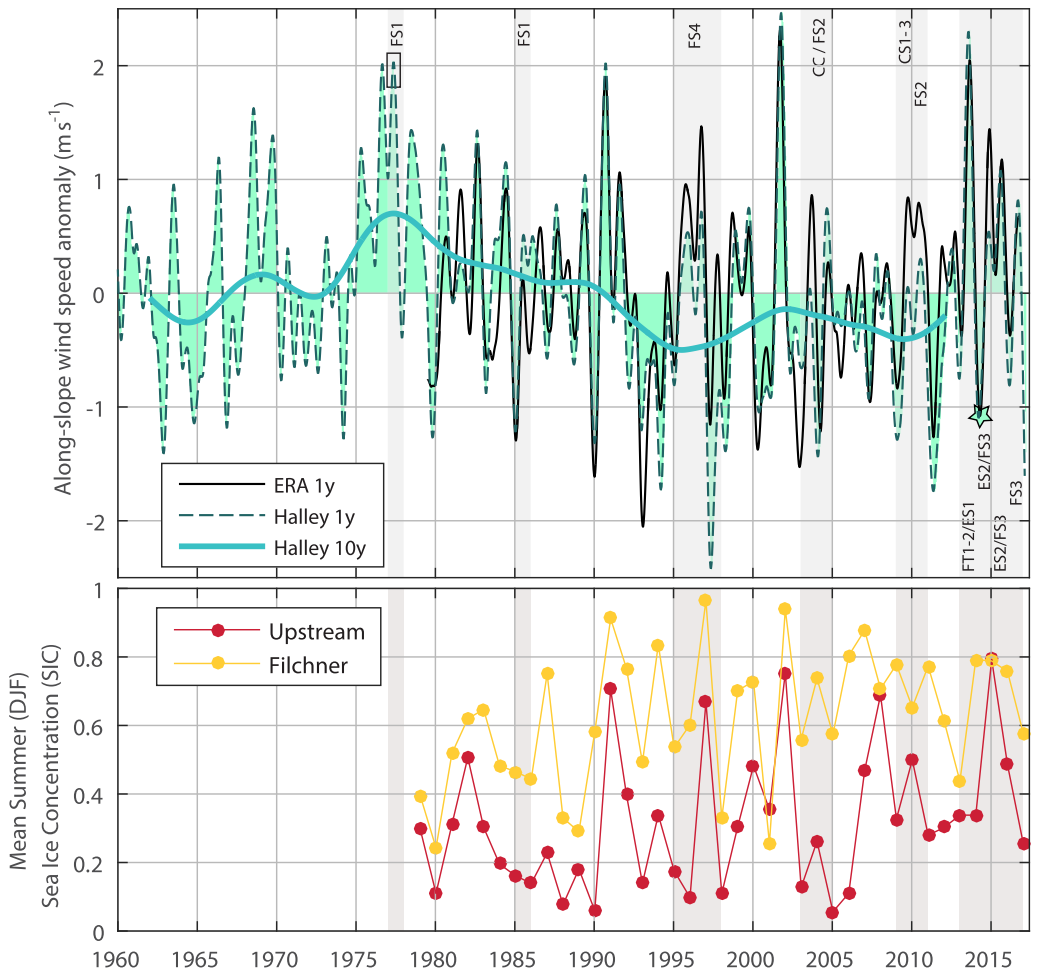

Figure 3. (a) Yearly low-passed wind speed anomaly toward 245° measured at Halley (filled, dashed turquoise) and from ERA averaged in the upstream area (black). The thick turquoise line shows 10 years low-passed wind at Halley, where the period after 2012 is omitted due to filter edge effects. (b) Summer Sea Ice Concentration from the Upstream area (red) and the Filchner area (yellow) indicated in Figure 1. Years with available current moorings are indicated by gray shading, and corresponding mooring names. The square marks a period of high Halley wind speed discussed in section 3.2, and the turquoise star marks the low wind speed in 2014 discussed in section 3.3.

overflow from the Filchner Sill and Trough, and continuing with the eastern shelf (section 3.3), and the regions upstream of the Filchner area (sections 3.5 and 3.6). The implications of the results are discussed in section 4.

3.1. Atmospheric Forcing and Sea Ice Concentration

Figure 3 shows the alongslope wind speed anomalies from ERA and Halley from 1960 to present. The year-to-year variability is large in both data series, with standard deviations of 0.51 m s^{-1} for Halley and 0.73 m s^{-1} for ERA, from 1 year low-passed alongslope wind in the period 1979 to 2016. In the Halley data series, which covers more than five decades, we also find multidecadal variability.

The upstream wind (averaged over the region marked by red lines in Figure 1) is mostly directed along the continental slope (toward 245°), but for some years, there is pronounced cross-flow wind (toward NE) during austral summer (Figure S1 in the supporting information).

The upstream region is mostly covered with sea ice (SIC $>$ 0.8) between May and October. There is large interannual variability for the summer (DJF) SIC, ranging from ice-free conditions (SIC $<$ 0.2) to full sea ice cover (SIC $\sim$ 0.8). The mean summer SIC is 0.3, and the minimum SIC is found in mid-February (Figure 3b). In the Filchner region (marked by a yellow line in Figure 1), there is generally higher SIC throughout the

year, compared to the upstream region. The period with full sea ice cover lasts longer (April–November), with a mean summer SIC of 0.6.

The variability of the summer SIC in the Filchner region is likely connected to the wind. We find high summer SIC (DJF) following strong alongslope wind in the preceding months (OND), which could indicate sea ice drift into the region. The correlation between the OND wind and the summer SIC in the Filchner region is $R = 0.6^{99}$ (not shown).

3.2. Ice Shelf Water Overflow From the Filchner Trough and Sill

Here we present 15 days low-passed time series of ISW overflow from the Filchner Trough and Sill region, starting with the moorings located on the sill (FS1–3), followed by mooring FS4 just south of the sill, and moorings farther south in the FT (FT1–2).

Several current meter records are available between 1977 and 2017. We identify periods of significant positive correlation between upstream alongslope wind and overflow current speed in all records. The correlation varies largely from year to year (Table 1). The ISW overflow speed has also large interannual variability, seen both from consecutive years at one mooring deployment (e.g., FS2 in 2003–2004 or FS3, Figure 5), and from different deployments at the same location (FS1 and FS2).

The highest correlation between wind and ISW overflow is found at FS1 in 1977, with a correlation coefficient of $R=0.52^{99}$ (Table 1). Analysis over 100 days moving windows indicates high correlation from February to August (Figure 4b). In this period we find that (I) the wind is mostly directed along the slope, (II) the overflow speed is high, (III) there is high variability in the 16–64 day period band for wind (Halley) and current wavelet power, and (IV) the alongslope wind speed anomaly is particularly high, compared to other years (see square in Figure 3). The strong wind is persistently directed toward southwest, and agrees with the conditions for recirculation of the slope current in the idealized model results of Daae et al. (2017) (Figure 2b). The correlation ceases in September, when the wind direction shifts toward north at Halley (Figures 4a and 4b), and both wind speed and current overflow speed are reduced.

Wavelet amplitudes from Halley wind speed and FS1 overflow speed (Figures 4c and 4d) are similar between February and August, with coinciding red and blue patches (positive and negative numbers). When the correlation ceases in September, the energetic oscillations from the Halley wind speed record shift toward longer time scales, and the current variability in the 16–64 day period band weakens.

The characteristics I–III are typical for most periods with high correlation between upstream wind and ISW overflow speed on the Filchner Sill. Figures of each mooring at FS1–2 is presented in the supporting information.

Mooring FS3 recorded the longest time series from the Filchner Sill, covering 3 years of data, from early 2014 to early 2017. The vertical extent of the ISW layer ($\theta < -1.9$°C) at FS3 varies through the year, being thicker from September to January when ISW surrounds both temperature sensors (584 m/485 m, Figure 5c). The depth of the ISW layer does not seem to affect the periods of correlation, as we find significant correlation both during periods of thick ISW layer (e.g., October–December 2014) and thin ISW layer (e.g., April–June 2015, Figure 5b). Similar seasonal variability in the ISW layer thickness is also observed on the shelf east of the FT (Ryan et al., 2017) (Figure 7), where it is accompanied by changes in the current direction.

Wavelet amplitudes from FS3 overflow speed and upstream ERA wind stress (Figures 5d and 5e) show highest agreement in 2014, consistent with the higher correlation coefficient this year (Table 1). From October 2015 to July 2016, there is weak correlation between overflow speed and wind. The wavelet amplitude for FS3 overflow is very low during this period, and the structure differs from the structure of the wind stress wavelet amplitude. From April to July 2016 (austral winter), the overflow speed is very high, and the ISW layer is thick. This could be a result of changes in the flow of ISW from under the FIS, but is not a seasonal feature, as it is not observed in 2014 or 2015. The SIC is anomalously high from December 2014 to January 2015 (austral summer). However, we do not see any changes in the temperature or current records linked to this anomaly.

At FS4, just south of the Filchner sill, a 28 month long record is available. We find an overall agreement between the FS4 overflow speed and the upstream wind stress (Table 1 and Figure 6b). Near the bottom,

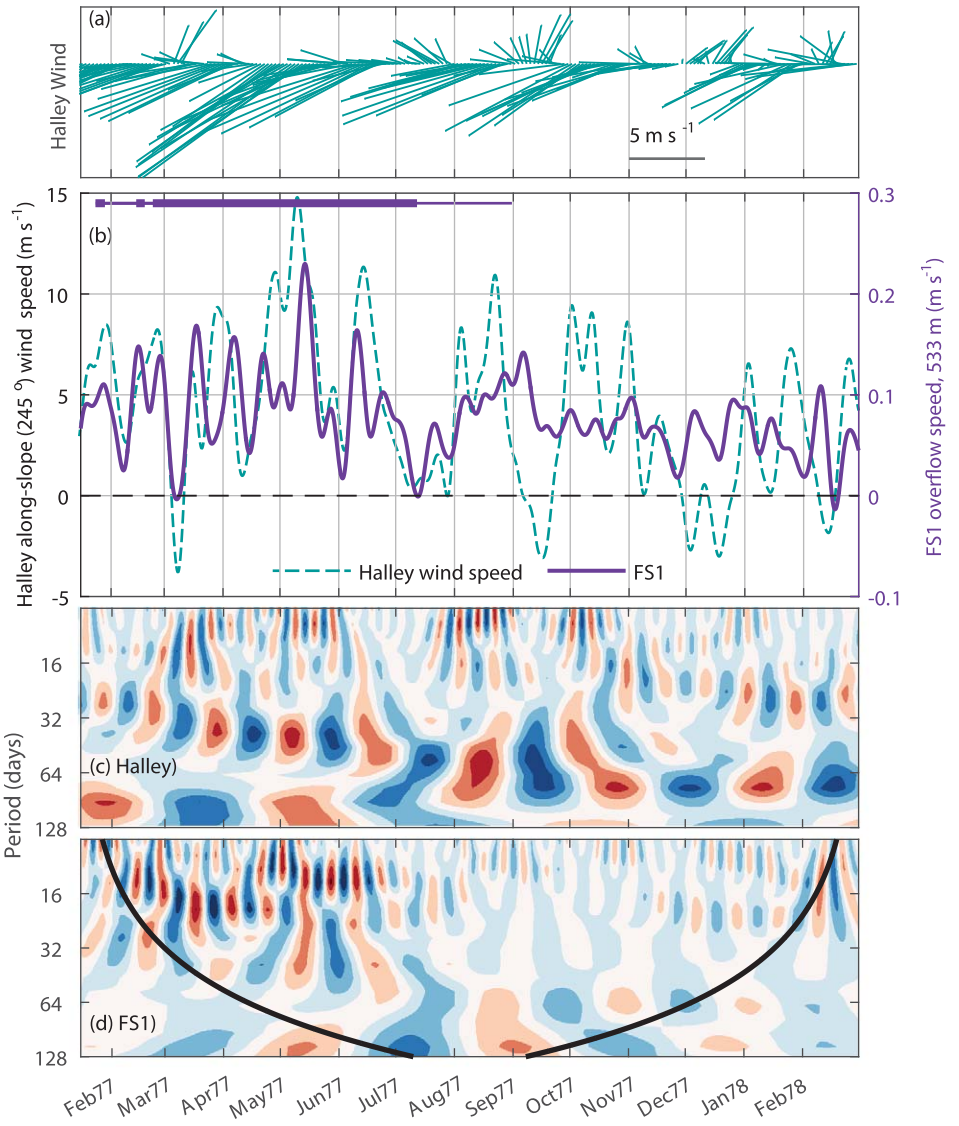

Figure 4. (a) Halley wind vectors, and (b) Halley along-flow wind speed and FS1 overflow speed in 1977. The horizontal bars in Figure 4b indicate periods of correlation between wind and current speed above the 95% significance level, identified from 100 days moving windows. The thick bars indicate the center point of each moving window, and the thin lines indicate the time span of the moving windows. Time series of the wavelet amplitudes (real part of the complex wavelet transform ($\mathrm{Re}(X_\omega)$) of (c) along-flow Halley wind speed, and (d) FS1 overflow speed. The color scale ranges from -7 to 7, and the thick black line in Figure 4d show the cone of influence from edge effects. Vertical ticks on the horizontal time axis are placed on the 15th day of the month throughout this manuscript.

and up to 378 m, there is ISW ($\theta < -1.9$°C) throughout the year (Foldvik et al., 2004). Analysis over 100 day moving windows shows high correlations between the overflow speed at 484 m and the upstream wind stress in 1995–1996. The windows with significant correlation are typically centered in periods with warm water present at 257 m (thick horizontal bars in Figure 6b). The warm water at 257 m, combined with strong alongslope wind, is suggestive of a RSC as sketched in Figure 2b. During periods of high correlation, we also find a good match between positive and negative (red and blue) patches of the wavelet amplitudes for wind stress and overflow speed (Figures 5d and 5e). Oscillations with 16–64 days periods occur in both time series in 1995, while also longer period oscillations (64–90 d) match in 1996.

The running correlation drops below the 95% significance level during austral summer, from December 1995 to February 1996. In this period, there is cold water high up in the water column, and the SIC is low in

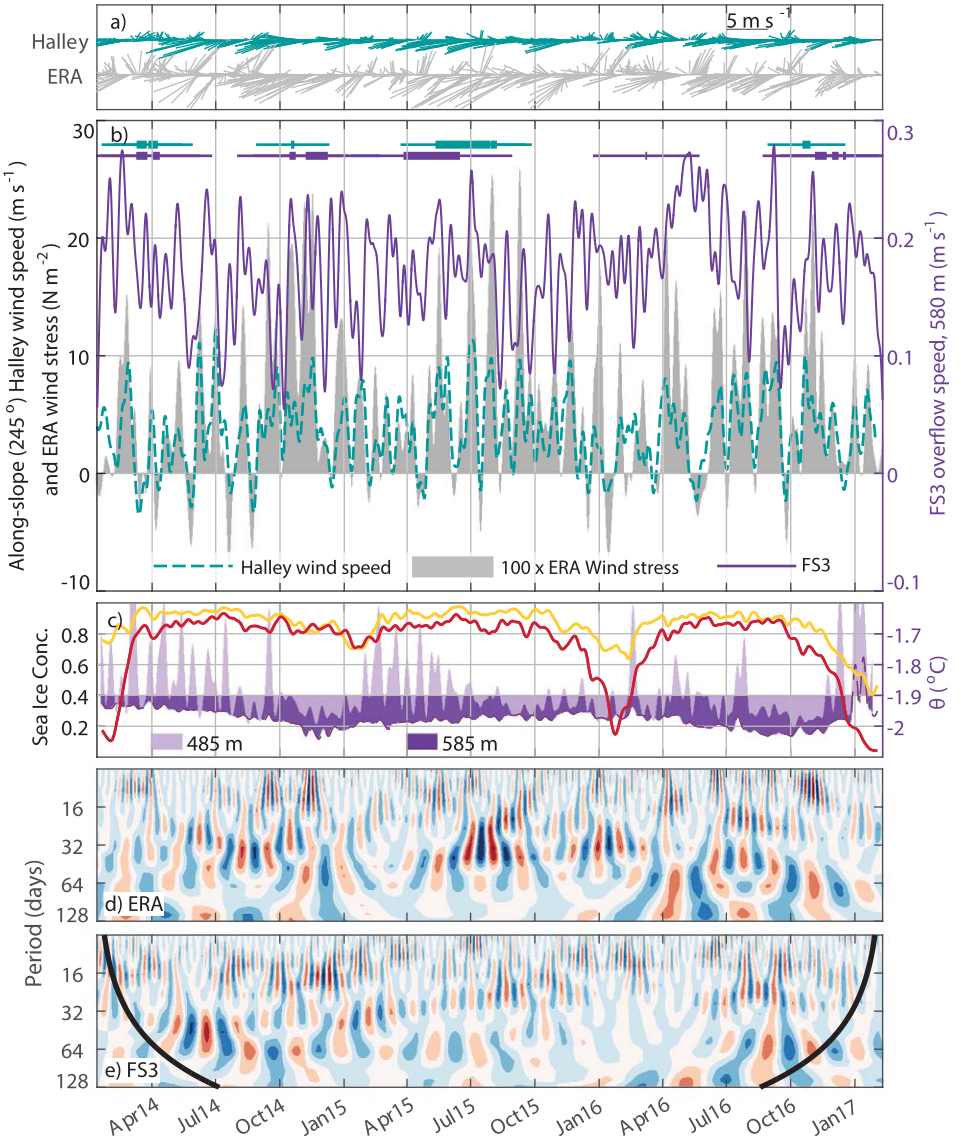

Figure 5. (a) Halley and ERA wind vectors. (b) Along-flow wind speed at Halley (turquoise) and wind stress from ERA (gray shade) together with FS3 overflow speed (purple) in 2014–2017. The horizontal bars in Figure 5b indicate periods of correlation between wind and current speed above the 95% significance level, identified from 100 days moving windows. We include Halley wind speed to show the similar results. (c) Temperature at 585 m (dark purple) and 485 m (light purple), and SIC averaged over the upstream slope area (red), and the Filchner area (yellow), according to Figure 1. The shading of the temperature curves highlights the freezing point of sea water at atmospheric pressure ($\theta = -1.9$°C). Time series of the wavelet amplitudes (real part of the complex wavelet transform (Re(X_ω)) of (d) along-flow ERA wind stress, and (e) FS3 overflow speed. The color scale ranges from −7 to 7, and the thick black line in Figure 5e show the cone of influence from edge effects.

the upstream area (Figure 6c). Wavelet amplitude patterns (Figures 6d and 6e) indicate that the oscillations in wind stress and overflow speed are out of phase. When the wind stress is weak, the overflow speed is anomalously high, with high variability at the shorter time scales (< 16 days), indicating current variability driven by other mechanisms than we study here. The results are similar to the observations from FS3 during the austral summer from December 2015 to February 2016.

The year 1997 stands out: the temperature maximum at 257 m is missing, suggesting that the seasonal inflow of MWDW was absent that year. Furthermore, we find ISW ($\theta < -1.9$°C) at all depths, summer SICs are anomalously high in both the upstream and the Filchner area, the wind forcing is weak, and there is no

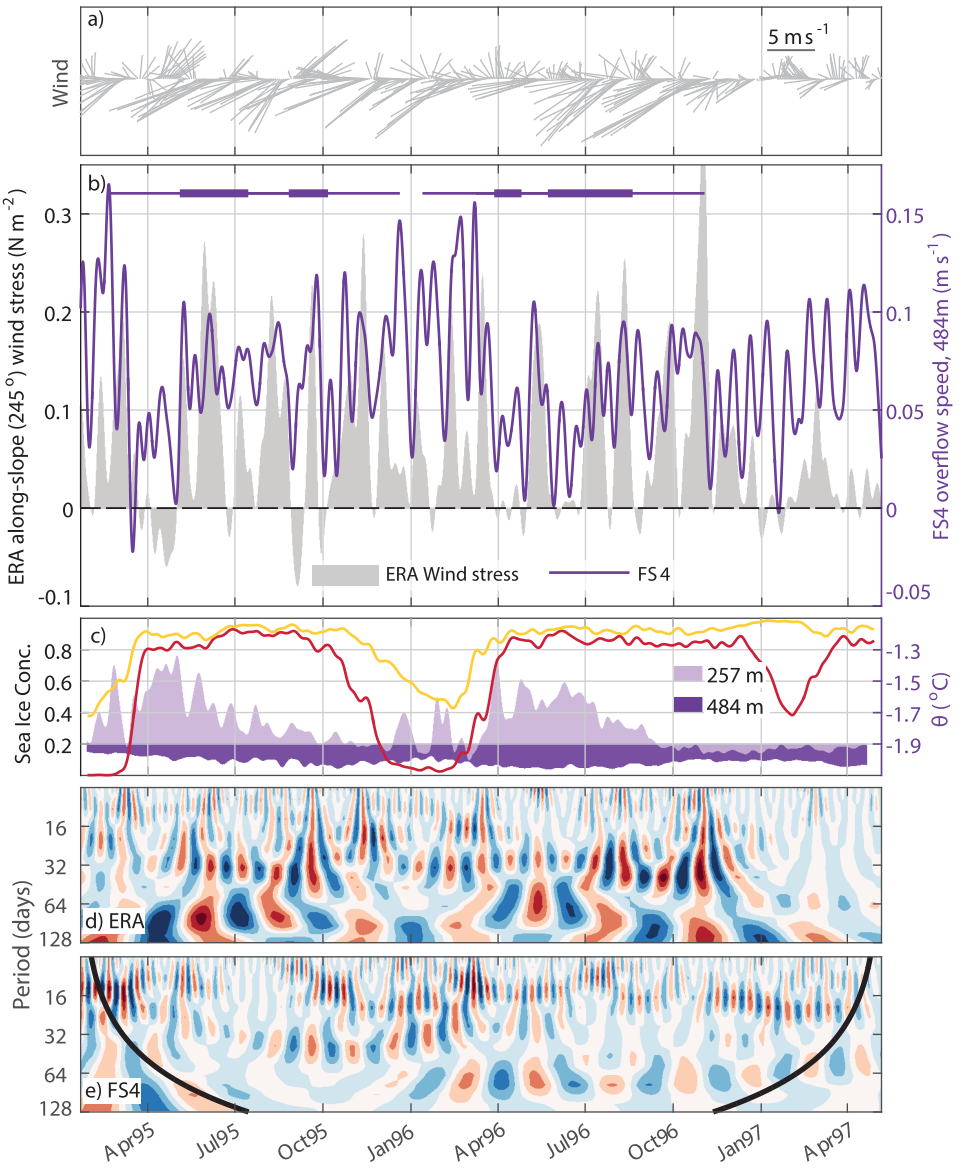

Figure 6. Same as Figure 5, but for the FS4 overflow speed (purple). Temperatures in Figure 6c are from 484 m (dark purple) and 257 m (light purple). We omit wind speed from Halley.

correlation between the upstream wind and the overflow at 484 m (Figures 3 and 6). Weak wind, and cold water at the upper instrument are consistent with the weak wind regime, as illustrated in Figure 2a, where no recirculation of the slope current occurs.

Further south in the FT (FT1–2), correlations between outflow speed and wind stress are nonsignificant for full records (Table 1). At FT1, analysis over 120 day moving windows indicates one longer period of significant correlation from February to May 2013, when warm water ($\theta < -1.9$°C) is present, and the wavelet amplitude patterns indicate similar oscillations in the period band 32–64 days (Figure 6 in SI). At FT2, there is only a short period with significant correlation (first part of February 2013), when the wavelet amplitudes from ERA wind stress and FT1 outflow are similar in the period band 16–32 days (Figure 5 in supporting information). During the rest of the time series, the wavelet amplitudes appear to be out of phase.

3.3. The Eastern Shelf

Here we present data from moorings on the upper eastern flank of the FT (ES1) and on the flat shelf, east of the FT (ES2), where a strong seasonality in both hydrography and circulation is observed (Ryan et al., 2017).

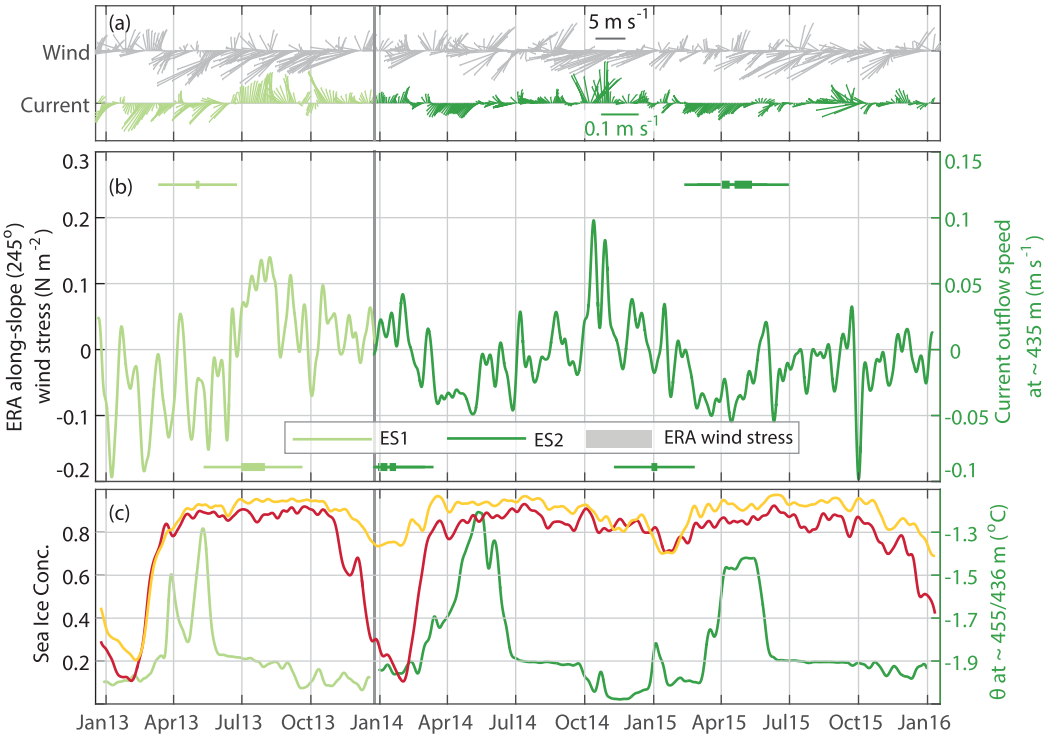

Figure 7. Same as Figure 6, but for ERA wind stress and current outflow speed at ES1 (light green) in 2013, and ES2 (dark green) in 2014–2015, both at 435 m depth. In Figure 7b, horizontal bars at the top, indicate running windows with positive correlations above the 95% significance level, while horizontal bars at the bottom indicate negative correlations. SIC in Figure 7c is averaged over the upstream slope area (red), and the Filchner area (yellow), according to Figure 1.

Inflow of Modified Warm Deep Water (MWDW) occurs from January to June, when the thermocline at the shelf break is shallow (Årthun et al., 2012; Darelius et al., 2016).

Two moorings on the shelf (green markers in Figure 1) show similar seasonal flow patterns, with presence of warm water during the inflow phase (Ryan et al., 2017) (Figure 7). A thorough discussion of the seasonality on the shelf is given in Ryan et al. (2017). The two mooring records from consecutive years are not colocated (separated by 132 km).

At ES1, the mean current is directed southward from January to July. We find significant (>95%) positive correlation with wind stress from late March when the SIC reaches 0.8, to July when the current changes direction. In this period, warm water ($\theta < -1.9$°C) surrounds the mooring, and correlation between wind and current on shorter (2–5 days) timescales are observed (Darelius et al., 2016). At ES2 the pattern is similar, although the correlations are weaker in 2014 (90–95% significance) compared to 2015. The weak correlation can possibly be explained by large variations in wind direction in 2014, compared to 2013 and 2015, and the strong minimum in 1 year low-passed wind speed (turquoise star in Figure 3). In 2015, the inflow period extends beyond July, and we find positive correlations both in March–July, when warm water is present, and in September–November when the mooring is surrounded by ISW.

At both moorings, negative correlations occur when the mean current is directed northward and ISW is present (Figures 7a and 7b). We also note high alongslope wind speed during spring (OND) 2013 and 2014, and high SIC in the succeeding summers (2014 and 2015), a relation which is described in section 3.1.

3.4. Recirculation of MWDW in the Filchner Trough

Moorings on the eastern shelf (ES1–2) show flow of MWDW ($\theta < -1.7$°C) toward the FIS cavity during summer and autumn (Darelius et al., 2016; Ryan et al., 2017). MWDW is also commonly observed in the FT in summer hydrographic sections, typically overlaying the ISW (Darelius et al., 2014a; Foldvik et al., 1985a; Nicholls et al., 2009).

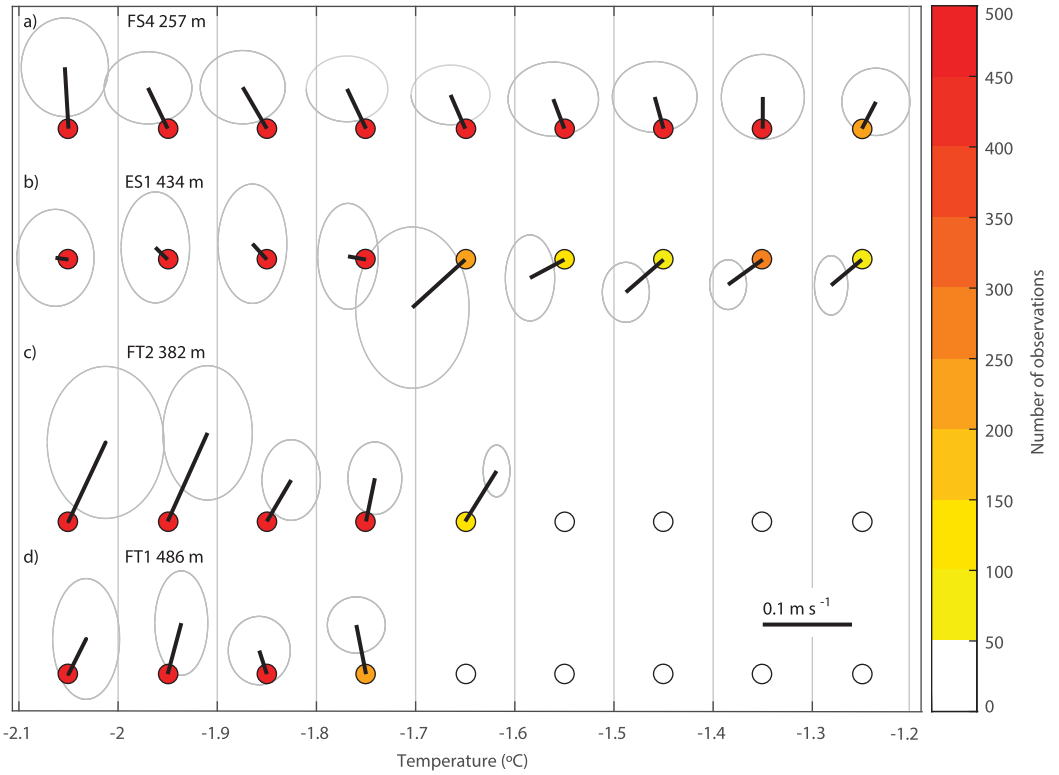

Figure 8. Mean velocity as a function of temperature in bins of 0.1°C intervals) at (a) FS4 257 m depths, (b) ES1 with velocity (θ) from 434 m (455 m) depth, (c) FT2 from 382 m (355 m) depth, and (d) FT1 from 486 m (475 m) depth. The colors indicate number of observations in each temperature bin, and the velocity scale is given in plot (d). The ellipses show the standard deviation of the detided velocity in the *x* directions and *y* directions.

Observations from FT2 and FS4 show that the MWDW observed here flows northward, following the ISW toward the sill (Figure 8). At these locations, the mean velocity has a northward component for all temperature ranges. At FT1, the low-passed temperature at 475 m depth does not exceed the −1.7°C threshold for MWDW. MWDW is found in the upper temperature sensors from 375 to 425 m (Darelius et al., 2016), but current records do not exist in this depth range. However, the warmest water at 475 m flows northward similar to what we find at FT2. At ES1, on the eastern flank of FT, the warmest water flows southward toward the FIS, while water with temperature below −1.7°C is directed toward west and nothwest, toward the FT.

The observations suggest that the MWDW flowing southward above the shallower isobaths and on the continental shelf in the east, to some extent recirculates and returns northward, away from the ice shelf cavity. The recirculation of MWDW is not to be confused with the RSC, described earlier, but could link the current variability in the FT to the wind and current variability observed over the continental shelf break.

3.5. Processes Along the Continental Slope

Three moorings (CS1–3) from the continental slope in 2009, are situated within the ASF (red markers in Figure 1). Away from the surface layer, the current is bottom-intensified. Since we are interested in slope-shelf interactions, we select current records from depths roughly corresponding to the shelf depth (approximately 250 m at CS1–2 and 400 m at CS3).

In 2009, the slope current is strongly related to the alongslope wind stress. The highest correlation is found at CS1 ($R = 0.69^{99}$ using full records, Table 1). At CS3, close to the FT opening, the correlation is depth-dependent, with higher correlation at 220 m depth compared to 400 m. At 400 m depth, the correlation is highest during March–July, when the current speed is high, the pycnocline is deep, and the wind and current wavelet amplitudes for oscillations with 16–64 day periods are large, indicating a more energetic driving force (Figure 9).

The SIC in 2009 (not shown) is similar to the SIC in 2003 and 2004 (Figure 10c), with high values (SIC $>$ 0.8) from March to November.

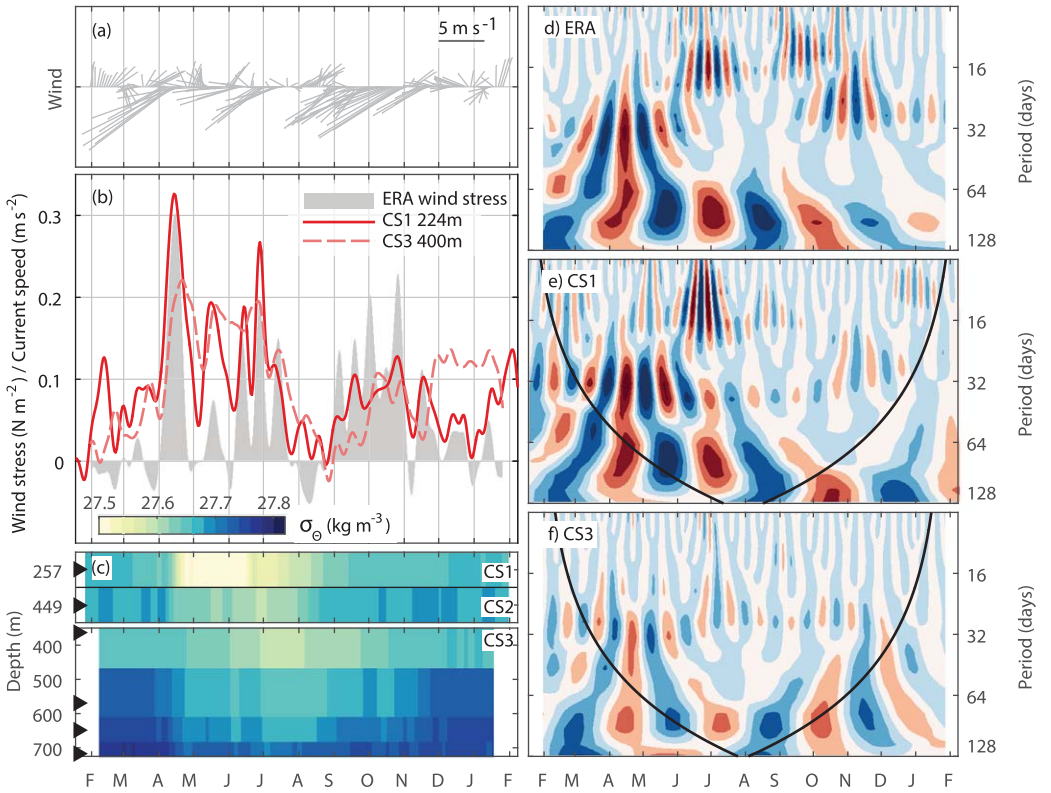

Figure 9. Time series of (a) Wind velocity from ERA Interim, (b) 15d low-passed along-flow ERA wind stress and along-flow current speed at CS1 (red solid line) and CS3 (red dashed line), and (c) potential density, σ_Θ,at CS1–3 in 2009. Time series of the Real part of the complex wavelet transform (Re(X_ω)) of Figure 9d alongslope wind speed, (e) along-flow current speed at CS1, and (f) along-flow current speed at CS3. The color scale ranges from −7 to 7, and the thick black lines in Figures 9e and 9f show the cone of influence from the edge effects.

The wavelet amplitudes for wind and current (Figures 9d–9f) have similar patterns, with strong power at low frequencies (period, $T > 64$ days) throughout 2009. The oscillation patterns for $T > 16$ days, and the alternating positive/negative amplitudes (red/blue patches) coincide in time, indicating that the oscillations are in phase. The wavelet amplitudes on the period band 16–64 days indicate more energetic oscillations from March to July, when the current speed is high. In this period, the slope current is also more barotropic (Núñez-Riboni & Fahrbach, 2009) and the volume transport is higher (Graham et al., 2013).

3.6. The Antarctic Coastal Current

The slope current bifurcates around 27°W (Heywood et al., 1998). The ACoC branch is directed southward, and roughly follows the coast of the Brunt Ice Shelf. Existing current data from CS and CC are from different time periods. Hence, we cannot assess directly how the upstream ASF affects the ACoC. However, the CC current data set comprises more than 2 years of recorded current, and therefore enables analysis of the year-to-year variability and possible connections to the ASF.

The current variability at CC is largely wind-driven ($R = 0.57^{99}$, Figure 10 and Table 1). The wind and current correlation is higher in 2003 compared to 2004. This is opposite to what we find at FS2, where the correlation with wind is highest in 2004. Correlations obtained from 150 days moving windows exceed the 95% confidence limit continuously from May to December 2003 (horizontal bars in Figure 10b). In 2004, the running correlations are significant in several shorter periods.

Wavelet analyses of current speed and wind stress reveal two differences between the first and the second deployment year (Figures 10d and 10e). First, the spectral energy is distributed differently. In 2003, the total energy for both wind and current is weaker than in 2004. Most of the energy is at low frequencies ($T > 64$ days), although power is also seen in the 16–32 day period band around September. In 2004, strong

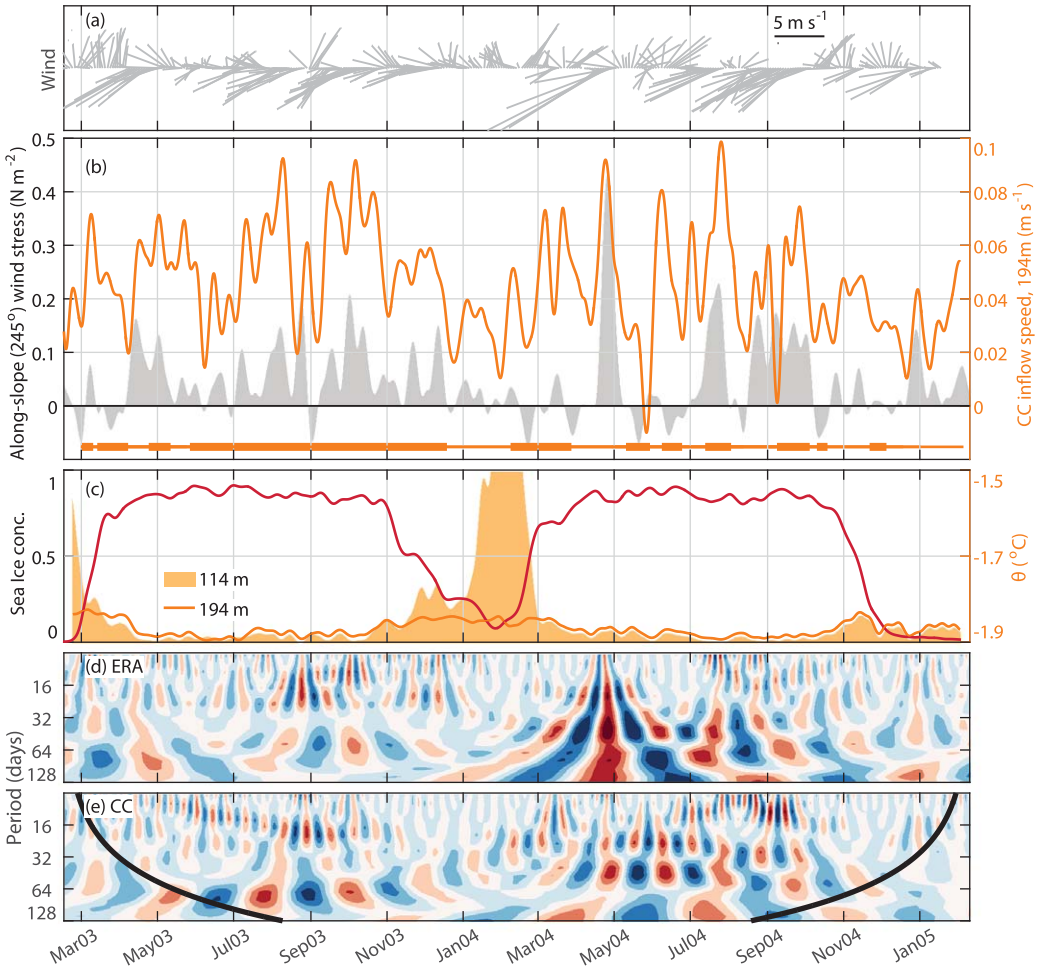

Figure 10. Time series of (a) ERA wind velocity, and (b) 15 day low-passed along-flow ERA wind stress (gray shade) and inflowing current speed at CC (orange). The horizontal bars in Figure 10b indicate periods of correlation between wind and current speed above the 95% significance level identified from moving windows of 150 days. The thick bars indicate the center point of each moving window, and the thin lines indicate the time span of the moving windows. (c) Sea Ice concentration from the slope (indicated by red curve in Figure 1) and potential temperature at 194 m (orange line) and 114 m (light orange shade). The temperature axis is cut at −1.5°C to increase the resolution of the lower temperature sensor. The upper temperature reach a peak of −1.26°C during late February 2004. Real part of the complex wavelet transform (Re(X_ω)) of Figure 10d alongslope ERA wind speed, and (e) inflowing current speed at CC. The thick black line in Figure 10e shows the cone of influence from edge effects.

oscillations are found at all displayed frequencies ($T \sim$ 8–128 days), and could be the result of strong storm activity. We note a strong storm event in May 2004, associated with high wavelet power at all frequency bands (Figure 10d). The storm event lasts approximately 10 days with associated alongslope wind speed above 10 m s^{-1} throughout the event, and a maximum of 25 m s^{-1}. Second, the wavelet amplitudes for wind and current are in phase for all frequencies in 2003, i.e., positive/negative amplitudes (red/blue patches) occur at the same time, while this is only true for oscillations with $T < 64$ days in 2004. In February 2004, when there is low SIC and a warm surface layer (Figure 10c), low-frequency oscillations ($T > 64$ days) appear in both time series. However, the oscillations are not in phase. This could explain the reduced correlation, despite the strong 16–64 day period oscillations present in both time series.

4. Discussion

The southeastern Weddell Sea is a remote region where observations are scarce. The data set compiled and presented in this study are from moorings deployed at various key locations, but typically in different years. The lack of concurrent sampling limits our ability to link mechanisms of forcing to circulation patterns.

Nevertheless, important insight is gained from the analysis with implications on the regional circulation patterns and the response to wind forcing at monthly time scales.

The slope current has previously been shown to respond to the seasonal cycle of the wind forcing along the continental slope (e.g., Fahrbach et al., 1992; Graham et al., 2013; Núñez-Riboni & Fahrbach, 2009). Sverdrup (1953) suggested that the on-shore Ekman transport, associated with wind from the east, builds up a pressure gradient toward the coast that leads to a stronger slope current. Here we show that a similar relation exists on monthly time scales. We find significant positive correlations between the monthly scale alongslope wind variability and the along-flow current variability on both the continental slope and along the Brunt Ice Shelf, in the ACoC pathway (Figures 9 and 10).

The ACoC crosses the shelf break where the continental shelf widens up around 27°W (see Figure 1). During periods of high along-flow wind speed, the ACoC speed is also high. This could indicate a higher water exchange between the continental slope and the shelf, but cannot be confirmed with only a single observation point. The amount of heat transported by the ACoC depends on the water masses associated with the transport. The majority of the heat is carried by solar heated surface water that accumulates along the coast (Sverdrup, 1953). At CC, we observe warm water in the upper layer during summer (Figure 10c). However, this water is likely too light and located too high up in the water column to enter the ice shelf cavity. Closer to the bottom at CC (194 m), the temperature increases slightly during summer, and both the current speed and the correlation with wind stress is weaker. This is likely related to a strong cross-flow wind speed component (toward NW). Cross-flow wind is common during summer, but does not occur every year.

The low-frequency wavelet amplitudes for wind stress and CC current shifts out of phase from summer 2004, and throughout the year (Figures 10d and 10e). During summer, the SIC is low and the wind stress is weak. Although the record at CC do not cover the full summer season in 2003 and 2005, it indicates a seasonal signal in temperature, with higher temperatures during summer in all years. The summer conditions are therefore similar in 2003 and 2004, and cannot explain why the low-frequency wavelet amplitudes shift out of phase in 2004, and not in 2003.

Darelius et al. (2016) suggested that the seasonal inflow of MWDW in the FT is a two-step process. First, warm water is lifted onto the shelf, and second, warm water present on the shelf can be transported south during favorable wind conditions (wind toward southwest). If MWDW comes into contact with the ice shelf, enhanced basal melting is expected. The MWDW flowing southward along the eastern flank of the FT is observed to recirculate and return northward in the FT (Figure 8). This inflow and recirculation of MWDW occur seasonally, and is not to be confused with the recirculation of the slope current in the sill area. The southward extent of the MWDW inflow recirculation may vary from year to year. MWDW was observed at FT1–2 in 2013, but was absent near the FIS in 2011 (Darelius et al., 2016). This could be explained by differences in wind forcing in 2011 and 2013. Dense water masses present on the shelf could also affect the southward transport of MWDW. In March–July, when the warm inflow is observed at ES1–2, the ISW layer does not reach the eastern shelf (Ryan et al., 2017). The thickness of the ISW layer could explain the seasonality of the flow direction in ES1–2. While a thin ISW layer allows southward flow of warm water, a thick layer could block the southward flow, and aid a westward redirection of the current. In order to quantify and monitor the southward heat flux in the FT and on the eastern shelf, one has to quantify the recirculation of MWDW, or place the moorings so far south that the recirculation occurring south of the mooring array is negligible.

In the FT and over the Filchner sill, we find unexpectedly strong correlation between the dense ISW overflow speed and the alongslope wind stress on monthly time scales. This connection implies that changes in the atmospheric circulation could affect the production rates of Antarctic Bottom Water, through changes in the overflow properties, and associated mixing rates with ambient water masses.

Wang et al. (2012) showed that, on seasonal scales, the Filchner export responds to onshore density anomalies caused by wind-induced variation of the isopycnal depression at the coast, with a lag of about 1 month. The observed variability of the overflow in the FT and sill reported here, responds to wind variability on the continental slope with no, or very short lags (less than 7 days). The mechanism for this covariability is different from the one described by Wang et al. (2012).

We do not have sufficient data to calculate the volume transport of the ISW overflow. The observed current speed variability could result from changes in the shape and/or position of the overflow current. Since we

do not have simultaneous observations from the continental slope and the overflow we cannot verify a link between the slope current and the overflow, or that recirculation of the slope current occurs. However, we do find higher correlations in periods when there is strong alongslope wind, combined with the presence of warm water (MWDW) in the upper water column (e.g., Figure 6), which could indicate that recirculation occurs (Daae et al., 2017). In 1997 (FS4), there is no indication of recirculation when the wind speed and its variability is weak, consistent with the modeled weak wind regime in Daae et al. (2017). At FT1–2, we only find short periods of correlation between wind and outflow speed. This indicates that either (I) the influence of monthly scale wind variability does not reach this far south, or (II) the wind forcing was not sufficient to drive a strong recirculation, as observed at FS4 in 1997. We suggest that (I) is the most likely reason, since the alongslope wind speed was high during most of the year (2013).

At FS1–4, we find large year-to-year variability in the correlation between wind and current speed for both consecutive years from multiyear deployments (FS2 in 2003–2004 and FS3 in 2014–2016), and for deployments at the same location in different years (FS1 and FS2). In addition to the interannual variability in the wind forcing (section 3.1), the Filchner Sill area is affected by several forcing mechanisms such as continental shelf waves (Jensen et al., 2013; Middleton et al., 1982; Semper & Darelius, 2017), tides (Fer et al., 2015; Pereira et al., 2002), SIC, and variability in the outflow of cold, dense, shelf water from underneath the FIS. Variability related to these mechanisms could be affecting the recirculation of the slope current. It is therefore likely that recirculation, and hence the link between ISW overflow speed and alongslope wind stress, is strongest in periods when the wind forcing at low frequencies is the dominating source of variability.

In several mooring deployments at FS1–4, we find significant correlation between wind and current speed during autumn, which ceases during winter. Although the results are not conclusive, this could indicate that recirculation of the slope current is strongest when the slope current is strong and barotropic (March–June, section 3.5, Núñez-Riboni & Fahrbach, 2009). Other mechanisms such as continental shelf waves, weaker wind forcing, or a cross-flow wind direction could also influence the slope current and recirculation.

The highest correlation between the alongslope wind and overflow speed at the Filchner sill is found at FS1 in 1977. Here, the alongslope wind forcing is strong, and we find high anomalies for both 1 and 10 year low-pass filtered Halley wind speed (Figure 3a). In the past few decades, atmospheric conditions in the southern high latitudes have been changing (Thompson & Solomon, 2002). The Southern Annular Mode (SAM) is thought to be the primary driver of such long-term climate variability (Thompson & Wallace, 2000). The SAM index is calculated from the difference in mean sea level pressure (mslp) between 40°S and 65°S. A positive SAM index is connected to a stronger cyclonic wind stress and spin-up of the Weddell gyre. Since the late 1970's, the SAM index has been increasing (Marshall, 2003), likely as a result of stratospheric ozone depletion and greenhouse gas emissions (Gillett & Thompson, 2003; Polvani et al., 2011). We find no significant correlation between the SAM index and the alongslope wind speed (245°) at Halley or in the continental slope region. However, the effect of SAM is most pronounced in multidecadal time scales, and the period we are studying might be too short to evaluate the effect of SAM directly. We do find a weak long-term wind variability in 1980–1990, when the SAM index is close to zero (not shown), but instead of increased wind speed since the 1970's, we note a long-term weakening of the alongslope wind speed from 1977 to 2010 (Figure 3a).

In addition to the SAM, the Semi-Annual Oscillation (SAO) affects the annual cycle of pressure and wind in the high southern latitudes. SAO results from differing annual cycles of temperature in the midlatitude ocean and the Antarctic regions (Meehl, 1991; Simmonds & Jones, 1998; Van Loon, 1967). SAO causes a poleward shift of the circumpolar trough in spring (September) and autumn (March), with associated higher meridional pressure gradients and surface wind stress (Hurrell & Loon, 1994). The amplitude of SAO is highest between 55°S and 65°S (Large & Loon, 1988). Unlike SAM, the phase of SAO is consistent from year to year, and is therefore thought to influence the long-term mslp more strongly than SAM at high latitudes (Hurrell & Loon, 1994). The SAO was particularly strong in the late 1970s, but has since been declining, likely caused by seasonal temperature changes in connection with SAM (Marshall, 2003; Van Loon et al., 1993). The observed long-term negative trend in alongslope wind speed at Halley (Figure 3) is consistent with the reduction of SAO. We speculate that the high correlations between wind and overflow at the Filchner Sill at FS1 in 1977 could be connected to strong SAO, and the reduced correlations found in later records, could partly be caused by decreased effects of SAO. However, the current data set is not sufficient to test whether the wind-current correlation is affected by the variability in SAO.

5. Conclusions

Observations of ocean currents and temperature from 14 moorings in the southeastern Weddell Sea are analyzed. We find significant correlation between the ISW overflow speed in FT and the alongslope wind stress over the upstream continental slope, which could have implications for the production rates of AABW. During strong northeasterly winds, we identified current records consistent with the recirculation of the slope current (RSC) at the mouth of the FT, as shown in the idealized numerical model results of Daae et al. (2017). We suggest that the RSC could explain the correlation between the wind stress and the overflow, however, in order to firmly establish whether recirculation of the slope current occurs, an array of moored instruments is needed over the Filchner Sill, covering both the RSC and the ISW overflow.

The variability in the slope current and the ACoC is strongly wind-driven on monthly time scales. Few measurements of the ACoC exist, and the amount of heat transported onto the shelf by the ACoC is still unknown. Our findings show that an increased wind stress along the continental slope leads to an increased current speed within the ACoC. Strong wind forcing, coinciding with a thin thermocline could therefore lead to large heat transports onto the shelf and contribute to basal melting of ice shelves. Similarly, the seasonal inflow and recirculation of MWDW to the eastern shelf is partly wind-driven. Long-term changes in the atmospheric forcing can alter the present situation characterized by weak and seasonal MWDW inflow, and possibly increase the heat transport onto the shelf region.

Acknowledgments

This work is supported by the Centre for Climate Dynamics at the Bjerknes Centre and by the Norwegian Research councils FRINATEK program through the project WARM (231549) and through the NARE program under the project WEDDELL (211415). For deployment and recovery of moorings, we would like to thank AWI, BAS, NP, and the crew and scientists on RV Polarstern (cruises PS08, PS34, PS82, grant AWI_PS82_02, PS96, grant AWI_PS96_01), RRS Ernest Shackleton (cruises ES006, ES033, ES052, ES060), RRS James Clark Ross (cruises JR097, JR244, JR16004), M/V Polarsirkel (NARE1, NARE2), K/V Andenes (NARE3), and HMS Endurance. We thank two anonymous reviewers for constructive comments that helped improve the manuscript substantially. The CS1–2 mooring data were provided by Karen Heywood at the University of East Anglia, and were funded by Antarctic Funding Initiative grant R14937 from the Natural Environment Research Council as the UK contribution to the SASSI program for the International Polar Year. A complete list of mooring data availability is given in supporting information. Wavelet software was provided by C. Torrence and G. Compo, and is available at URL: http://paos.colorado.edu/research/wavelets/

References

Andreas, E. L., Horst, T. W., Grachev, A. A., Persson, P. O. G., Fairall, C. W., Guest, P. S., et al. (2010). Parametrizing turbulent exchange over summer sea ice and the marginal ice zone. *Quarterly Journal of the Royal Meteorological Society*, *136*(649), 927–943. https://doi.org/10.1002/qj.618

Årthun, M., Nicholls, K. W., Makinson, K., Fedak, M. A., & Boehme, L. (2012). Seasonal inflow of warm water onto the southern Weddell Sea continental shelf, Antarctica. *Geophysical Research Letters*, *39*, L17601. https://doi.org/10.1029/2012GL052856

British Antarctic Survey (2013). *UK Antarctic surface meteorology; 1947–2013, Database, Version 1.0*. Cambridge, UK: Polar Data Centre, British Antarctic Survey.

Carmack, E. C., & Foster, T. (1977). Water masses and circulation in the Weddell Sea. In M. J. Dunbar (Ed.), *Proceedings of the polar ocean conference, Montreal, 1974* (pp. 151–165). Calgary, AB: Arctic Institute of North America.

Cavalieri, D., C.L, P., Gloersen, P., & Zwally, H. (1996). *Sea ice concentrations from Nimbus-7 SMMR and DMSP SSM/I-SSMIS passive microwave data, Version 1* (NSIDC-0051). Boulder, CO: NASA National Snow and Ice Data Center Distributed Active Archive Center. https://doi.org/10.5067/8GQ8LZQVL0VL

Cooper, G. R. J., & Cowan, D. R. (2008). Comparing time series using wavelet-based semblance analysis. *Computers & Geosciences*, *34*, 95–102. https://doi.org/10.1016/j.cageo.2007.03.009

Daae, K., Hattermann, T., Darelius, E., & Fer, I. (2017). On the effect of topography and wind on warmwater inflow—An idealized study of the southern Weddell Sea continental shelf system. *Journal of Geophysical Research: Ocean*, *122*, 2622–2641. https://doi.org/10.1002/2016JC012541

Darelius, E., Fer, I., & Nicholls, K. W. (2016). Observed vulnerability of Filchner-Ronne Ice Shelf to wind-driven inflow of warm deep water. *Nature Communications*, *7*, 1–7. https://doi.org/10.1038/ncomms12300

Darelius, E., Makinson, K., Daae, K., Fer, I., Holland, P. R., & Nicholls, K. W. (2014a). Hydrography and circulation in the Filchner Depression, Weddell Sea, Antarctica. *Journal of Geophysical Research: Oceans*, *119*, 5797–5814. https://doi.org/10.1002/2014JC010225

Darelius, E., Smedsrud, L. H., Østerhus, S., Foldvik, A., & Gammelsrød, T. (2009). Structure and variability of the Filchner overflow plume. *Tellus, Series A*, *61*(3), 446–464. https://doi.org/10.1111/j.1600-0870.2009.00391.x

Darelius, E., Strand, K. O., Østerhus, S., Gammelsrød, T., Årthun, M., & Fer, I. (2014b). On the seasonal signal of the Filchner Overflow, Weddell Sea, Antarctica. *Journal of Physical Oceanography*, *44*(4), 1230–1243. https://doi.org/10.1175/JPO-D-13-0180.1

Dee, D. P., Uppala, S. M., Simmons, A. J., Berrisford, P., Poli, P., Kobayashi, S., et al. (2011). The ERA-Interim reanalysis: Configuration and performance of the data assimilation system. *Quarterly Journal of the Royal Meteorological Society*, *137*(656), 553–597. https://doi.org/10.1002/qj.828

Fahrbach, E., Rohardt, G., & Krause, G. (1992). The Antarctic coastal current in the southeastern Weddell Sea. *Polar Biology*, *12*(2), 171–182. https://doi.org/10.1007/BF00238257

Fer, I., Müller, M., & Peterson, A. K. (2015). Tidal forcing, energetics, and mixing near the Yermak Plateau. *Ocean Science*, *11*, 287–304. https://doi.org/10.5194/os-11-287-2015

Foldvik, A., Gammelsrød, T., Østerhus, S., Fahrbach, E., Rohardt, G., Schröder, M., et al. (2004). Ice shelf water overflow and bottom water formation in the southern Weddell Sea. *Journal of Geophysical Research*, *109*, C02015. https://doi.org/10.1029/2003JC002008

Foldvik, A., Gammelsrød, T., & Tørresen, T. (1985a). Hydrographic observations from the Weddell Sea during the Norwegian Antarctic research expedition 1976/77. *Polar Research*, *3*, 177–193.

Foldvik, A., Gammelsrød, T., & Tørresen, T. (1985b). Physical oceanography studies in the Weddell Sea during the Norwegian Antarctic Research Expedition 1978/79. *Polar Research*, *3*(2), 195–207. https://doi.org/10.1111/j.1751-8369.1985.tb00507.x

Gill, A. (1973). Circulation and bottom water production in the Weddell Sea. *Deep Sea Research and Oceanographic Abstracts*, *20*(2), 111–140. https://doi.org/10.1016/0011-7471(73)90048-X

Gillett, N. P., & Thompson, D. (2003). Simulation of recent Southern hemisphere climate change. *Science*, *302*, 273–276.

Gordon, A. L., Huber, B., McKee, D., & Visbeck, M. (2010). A seasonal cycle in the export of bottom water from the Weddell Sea. *Nature Geoscience*, *3*(8), 551–556. https://doi.org/10.1038/ngeo916

Graham, J. A., Heywood, K. J., Chavanne, C. P., & Holland, P. R. (2013). Seasonal variability of water masses and transport on the Antarctic continental shelf and slope in the southeastern Weddell Sea. *Journal of Geophysical Research: Oceans*, *118*, 2201–2214. https://doi.org/10.1002/jgrc.20174

Grosfeld, K., Schröder, M., Fahrbach, E., Gerdes, R., & Mackensen, A. (2001). How iceberg calving and grounding change the hydrography in the Filchner Ice Shelf-Ocean System. *Journal of Geophysical Research*, *106*, 9039–9055.

Hellmer, H. H., Kauker, F., Timmermann, R., Determann, J., & Rae, J. (2012). Twenty-first-century warming of a large Antarctic ice-shelf cavity by a redirected coastal current. *Nature*, *485*(7397), 225–228. https://doi.org/10.1038/nature11064

Hellmer, H. H., Kauker, F., Timmermann, R., & Hattermann, T. (2017). The fate of the Southern Weddell Sea continental shelf in a warming climate. *Journal of Climate*, *30*, 4337–4350. https://doi.org/10.1175/JCLI-D-16-0420.1

Heywood, K. J., Locarnini, R. A., Frew, R. D., Dennis, P. F., & King, B. A. (1998). Transport and water masses of the Antarctic slope front system in the Eastern Weddell Sea. *Ocean, Ice, and Atmosphere—Interaction at the Antarctic Continental Margin*, *75*, 203–214.

Hurrell, J. W., & Loon, H. V. (1994). A modulation of the atmospheric annual cycle in the Southern Hemisphere. *Tellus, Series A*, *46*(3), 325–338. https://doi.org/10.3402/tellusa.v46i3.15482

IOC, SCOR, and IAPSO (2010). *The international thermodynamic equation of seawater—2010: Calculation and use of thermodynamic properties* (in English) (Manuals and Guides 56). Intergovernmental Oceanographic Commission, UNESCO.

Jacobs, S. (1991). On the nature and significance of the Antarctic Slope Front. *Marine Chemistry*, *35*(1–4), 9–24. https://doi.org/10.1016/S0304-4203(09)90005-6

Jensen, M. F., Fer, I., & Darelius, E. (2013). Low frequency variability on the continental slope of the southern Weddell Sea. *Journal of Geophysical Research: Oceans*, *118*, 4256–4272. https://doi.org/10.1002/jgrc.20309

Klinck, J. M. (1996). Circulation near submarine canyons: A modeling study. *Journal of Geophysical Research*, *101*(95), 1211–1223. https://doi.org/10.1029/95JC02901

Large, W. G., & Loon, H. V. (1988). Large scale, low frequency variability of the 1979 FGGE surface buoy drifts and winds over the south hemisphere. *Journal of Physical Oceanography*, *19*, 216–232. https://doi.org/10.1175/1520-0485(1989)019<0216:LSLFVO>2.0.CO;2

Lilly, J. (2017). *jLab: A data analysis package for matlab, v. 1.6.3*. Retrieved from http://www.jmlilly.net/jmlsoft.html

Marshall, G. J. (2003). Trends in the southern annular mode from observations and reanalyses. *Journal of Climate*, *16*(24), 4134–4143.

Maslanik, J., & Stroeve, J. (1999). *Near-real-time DMSP SSM/I-SSMIS daily polar gridded sea ice concentrations*. Boulder, CO: NASA DAAC at the National Snow and Ice Data Center.

Meehl, G. A. (1991). A reexamination of the mechanism of semiannual oscillation in the southern hemisphere. *Journal of Climate*, *4*, 911–926.

Middleton, J., Foster, T., & Foldvik, A. (1982). Low-frequency currents and continental shelf waves in the southern Weddell Sea. *Journal of Physical Oceanography*, *12*(7), 618–634.

Nicholls, K. W. (2005). *JR097 Cruise Report Autosub under ice cruise to the southern Weddell Sea* (technical report). Cambridge, UK: British Antarctic Survey.

Nicholls, K. W., Østerhus, S., Makinson, K., Gammelsrød, T., & Fahrbach, E. (2009). Ice-ocean processes over the continental shelf of the southern Weddell Sea, Antarctica: A review. *Reviews of Geophysics*, *47*, RG3003. https://doi.org/10.1029/2007RG000250

Nøst, O. A., & Østerhus, S. (1998). Impact of grounded icebergs on the hydrographic conditions near the Filchner Ice Shelf. *Antarctic Research Series*, *75*, 267–284.

Núñez-Riboni, I., & Fahrbach, E. (2009). Seasonal variability of the Antarctic Coastal Current and its driving mechanisms in the Weddell Sea. *Deep Sea Research, Part I*, *56*(11), 1927–1941. https://doi.org/10.1016/j.dsr.2009.06.005

Pereira, A. A. F., Beckmann, A., & Hellmer, H. H. (2002). Tidal mixing in the Southern Weddell Sea: Results from a three-dimensional model. *Journal of Physical Oceanography*, *32*(7), 2151–2170. https://doi.org/10.1175/1520-0485(2002)032<2151:TMITSW>2.0.CO;2

Polvani, L., Waugh, D., Correa, G., & Son, S. (2011). Stratospheric ozone depletion: The main driver of twentieth-century atmospheric circulation changes in the southern hemisphere. *Journal of Climate*, *24*(3), 795–812. https://doi.org/10.1175/2010JCLI3772.1

Pritchard, H. D., Ligtenberg, S., Fricker, H., Vaughan, D. G., van den Broeke, M., & Padman, L. (2012). Antarctic ice-sheet loss driven by basal melting of ice shelves. *Nature*, *484*(7395), 502–505. https://doi.org/10.1038/nature10968

Rignot, E., Jacobs, S., Mouginot, J., & Scheuchl, B. (2013). Ice-shelf melting around Antarctica. *Science*, *341*(6143), 266–270. https://doi.org/10.1126/science.1235798

Ryan, S., Hattermann, T., Darelius, E., & Schröder, M. (2017). Seasonal cycle of hydrography on the eastern shelf of the Filchner Trough,Weddell Sea, Antarctica. *Journal of Geophysical Research: Ocean*, *122*, 6437–6453. https://doi.org/10.1002/2017JC012916

Sciremammano, F. (1979). Suggestion for the presentation of correlations and their significance levels. *Journal of Physical Oceanography*, *9*, 1273–1276. https://doi.org/10.1175/1520-0485(1979)009<1273:ASftpO>2.0.CO;2

Semper, S., & Darelius, E. (2017). Seasonal resonance of diurnal continental shelf waves in the southern Weddell Sea. *Ocean Science*, *13*, 77–93. https://doi.org/10.5194/os-2016-36

Simmonds, I. A. N., & Jones, D. A. (1998). The mean structure and temporal variability of the semiannual oscillation in the southern extratropics. *International Journal of Climatology*, *18*, 473–504.

Sverdrup, H. (1953). The currents off the coast of Queen Maud Land. *Norsk Geografisk Tidskrift*, *14*, 239–249.

Thompson, D., & Solomon, S. (2002). Interpretation of recent southern hemisphere climate change. *Science*, *296*, 895–900.

Thompson, D., & Wallace, J. (2000). Annular modes in the extratropical circulation. Part I. *Journal of Climate*, *13*, 1000–1016.

Timmermann, R., & Hellmer, H. H. (2013). Southern Ocean warming and increased ice shelf basal melting in the twenty-first and twenty-second centuries based on coupled ice-ocean finite-element modelling. *Ocean Dynamics*, *63*(9–10), 1011–1026. https://doi.org/10.1007/s10236-013-0642-0

Van Loon, H. (1967). The half-yearly oscillations in middle and high southern latitudes and the coreless winter. *Journal of Atmospheric Sciences*, *24*, 472–486.

Van Loon, H., Kidson, J., & Mullan, A. B. (1993). Decadal variation of the annual cycle in the Australian dataset. *Journal of Climate*, *6*, 1227–1231.

Wang, Q., Danilov, S., Fahrbach, E., Schröter, J., & Jung, T. (2012). On the impact of wind forcing on the seasonal variability of Weddell Sea Bottom Water transport. *Geophysical Research Letters*, *39*, L06603. https://doi.org/10.1029/2012GL051198

Williams, W. J., Gawarkiewicz, G. G., & Beardsley, R. (2001). The adjustment of a shelfbreak jet to cross-shelf topography. *Deep Sea Research, Part II*, *48*(1–3), 373–393. https://doi.org/10.1016/S0967-0645(00)00085-0

Woodgate, R. A., & Schröder, M. (1998). Moorings from the Filchner Trough and the Ronne Ice Shelf Front: Preliminary results, *Filchner Ronne Ice Shelf Programme*, *12*, 85–90.

Zhang, Y., Pedlosky, J., & Flierl, G. R. (2011). Cross-shelf and out-of-bay transport driven by an open-ocean current. *Journal of Physical Oceanography*, *41*, 2168–2186. https://doi.org/10.1175/JPO-D-11-08.1